Fabrication of gas sensor based on field ionization from SWCNTs with tripolar microelectrode

2012 J. Micromech. Microeng. 22 125017

(http://iopscience.iop.org/0960-1317/22/12/125017)

J. Micromech. Microeng. **22** (2012) 125017 (6pp) doi:10.1088/0960-1317/22/12/125017

Fabrication of gas sensor based on field ionization from SWCNTs with tripolar microelectrode

Shengbing Cai[1], **Yong Zhang**[1] **and Zhemin Duan**[2]

[1] Department of Electrical Engineering, Xi'an Jiaotong University, No.28, Western Xianning Road, Xi'an, Shaanxi, People's Republic of China
[2] Department of Electronics and Information Engineering, Northwestern Polytechnical University, No.127, Western Youyi Road, Xi'an, Shaanxi, People's Republic of China

E-mail: caisb@sneac.edu.cn

Received 9 August 2012, in final form 5 October 2012
Published 6 November 2012
Online at stacks.iop.org/JMM/22/125017

Abstract
We report the nanofabrication of a sulfur dioxide (SO_2) sensor with a tripolar on-chip microelectrode utilizing a film of single-walled carbon nanotubes (SWCNTs) as the field ionization cathode, where the ion flow current and the partial discharge current generated by the field ionization process of gaseous molecules can be gauged to gas species and concentration. The variation of the sensitivity is less than 4% for all of the tested devices, and the sensor has selectivity against gases such as He, NO_2, CO, H_2, SO_2 and O_2. Further, the sensor response presents well-defined and reproducible linear behavior with regard to concentration in the range investigated and a detection limitation of $<\sim$0.5 ppm for SO_2. More importantly, a tripolar on-chip microelectrode with SWCNTs as a cathode exhibits an impressive performance with respect to stability and anti-oxidation behavior, which are significantly better than had been possible before in the traditional bipolar sensor under explicit circumstances at room temperature.

(Some figures may appear in colour only in the online journal)

1. Introduction

There is increasing demand for gas sensors in diverse applications, such as chemical and petroleum refining, automobile exhaustion, environmental monitoring, gas detection for counter-terrorism, etc. In view of these applications, some of the key attributes expected of a sensor including good sensitivity, low detection limit, fast response and recovery time, good specificity with low false positive and long term stability with a wide temperature operation range is also highly desirable [1]. Hence, various approaches are being investigated to develop these sensors [2–12]. Most commercially available sensors are made using semiconducting oxides as the sensing material. The main drawback of using oxide-based gas sensors is that their use in gas sensing is governed by microfabrication techniques used to manufacture the sensor. This puts a limit on the high working temperature, bulky architecture and high power consumption of sensor [2, 3]. Impedance sensors [4, 5] have an operating principle that underlines that the presence of various gases reversibly alters the impedance of some electrochemical systems in a repeatable fashion that can be correlated to concentration are discussed extensively in the larger context of solid state sensors including of amperometric and potentiometric varieties. The variety of sensors available holds promise for accurate gas detection on the single parts per million (ppm) level. However, selectivity, complicated supporting electronics and long-term stability remain critical challenges.

On the other hand, single-walled nanotubes (SWCNTs) stand out as a strong candidate for use as a gas sensing material due to their inherent properties such as small size (diameter $\sim$1–100 nm) and good electrical and mechanical properties. Another important property of nanotubes which favors their use in gas sensing is their high specific surface area $\sim$1580 m^2 g^{-1}). Indeed, gas sensors made from

semiconducting SWNTs are sensitized to NH_3, CO and NO_2 at room temperature and atmospheric pressure [10, 11]. There is a significant improvement over traditional counterparts which usually require heating to temperatures exceeding 350 °C. However, it is generally difficult to obtain semiconducting SWCNTs. Even when nanotubes are directly grown by chemical vapor deposition, there is no control over the growth of semiconducting or metallic tube's selectivity. This often results in fabrication complexity, low sensor yield and poorly reproducible sensor performance.

To overcome some of these limitations, the investigation reported here was undertaken with the view of introducing certain improvements into the electrode configuration of the miniaturized on-chip ionization gas sensors with SWCNTs film as field ionization cathode, and thus obtaining a higher sensitivity and selectivity than those of conventional bipolar systems under explicit environment. The tripolar microelectrodes sensor described here differs from other field ionization ones in that (1) the introduction of high quality SWCNTs can dramatically enhance the electric field on the surface and in the vicinity of the materials by a factor up to the order of 10^3–10^4 and thus significantly lower the onset voltage of gas discharges in comparison to the flat-metal-plate counterparts, (2) the introduction of an extraction sensing electrode that is supposed to improve electric field distribution uniform facilitates the involvement of electron exchange between cathode and collector electrode, which maintains the stability and anti-oxidation behavior of the sensor.

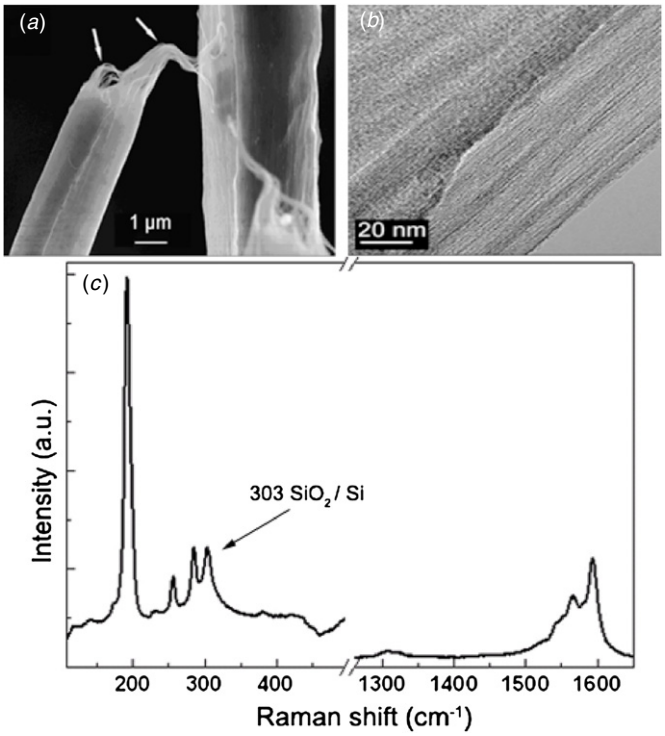

Figure 1. (*a*) SEM image of the vertically aligned SWCNTs array. The good flexibility is indicated by arrows. (*b*) TEM image of SWCNTs. (*c*) Raman spectrum of as-fabricated SWCNTs grown from Co–Mo catalyst with peaks at 303 cm^{-1} originating from Si/SiO_2 substrate and used for calibration, and the excitation laser is 632.8 nm.

2. Experimental details

2.1. Synthesis and characterizations

SWCNTs have been synthesized by the alcohol catalytic chemical vapor deposition method [13–15] on the surfaces of the Si or SiO_2 substrates.

More specifically, using alcohol as the precursor and bimetallic Co–Mo nanoparticles, large-area and uniform SWCNTs were prepared on a Si/SiO_2 substrate by the CVD process. The catalysts were dip-coated in turn using molybdenum and cobalt acetate solution (dissolved in alcohol) on both sides of the optically polished silicon substrate using electron-beam lithography to provide for the patterned growth of SWCNTs. For reduction of the acetate to metallic clusters, the dip-coated substrate was baked in air at 400 °C for 5 min. The reduced metals were then oxidized in air forming monodisperse nanoparticles 1–2 nm in diameter.

For the growth of SWCNTs films, a piece of substrate coated with Co–Mo catalysts was set in a tube furnace, which had been preheated to 800 °C with Ar/H_2 (3%) flow. Then the substrate was kept at 800 °C for extra 10 min to reduce the oxide catalysts. Subsequently, vaporized alcohol was injected into the furnace and the growth process immediately started. The pressure was maintained at ∼10 Torr. Finally, the substrates were naturally cooled to room temperature under Ar in the furnace [15]. During the whole synthesis process, the growth directions of the nanotubes can be controlled by van der Waals self-assembly forces or the pristine stress. Because the growth of SWCNTs is believed to occur via decomposition of the carbonaceous gas molecules at the catalyst particle surface, diffusion of carbon atoms through the particle, and subsequent precipitation at the particle/tubes interface. The axis of a CNTs growing perpendicular to substrate coincides with the direction of the applied stress and the entangled and poorly ordered SWCNTs are thus vertically aligned.

The sensing materials consists of SWCNTs purified using a two step purification procedure [16]. The as grown SWCNTs were purified with acid to remove the residuals of the metallic catalyst, followed by air oxidation at high temperature to remove the graphitic carbons. The final purified SWCNTs have a purity of >99.6% and a surface area of 1600 $m^2\ g^{-1}$. Such a high purity level is critical to ensure the sensor response from the nanotubes and is not affected by metal and amorphous carbon impurities.

The microstructures of the samples were characterized with transmission electron microscopy (FEI Tecnai F30, TEM) and the morphologies of the SWCNTs by scanning electron microscope (Hitachi S800, SEM). From the SEM and TEM images of the samples (shown in figures 1(*a*) and (*b*)), it is seen that the SWCNTs fabricated in this way are perfectly aligned, densely uniform distributed and relatively vertical to the Si substrate. Their average length is about ∼10 μm and the diameter is ∼50 nm. Further, the as-fabricated SWCNTs films grown from Co–Mo catalyst were characterized by micro-Raman spectroscopy with 632.8 nm laser excitation, as shown

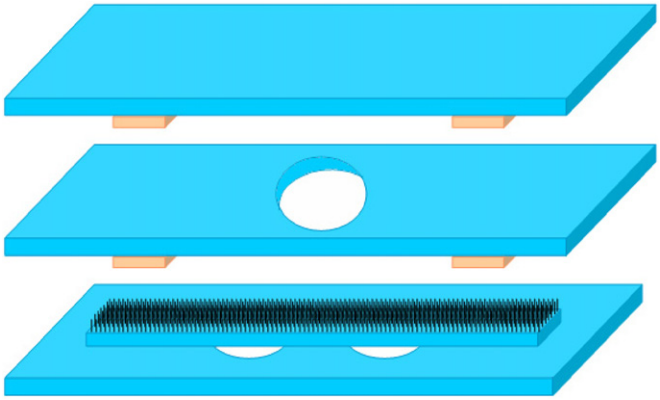

Figure 2. Schematic of the sensor.

in figure 1(*c*). The presence of the radial breathing mode is indicative of the high quality of the SWCNTs.

2.2. Fabrication of sensor

In the following section, the fabrication of the sensing electrodes is described using a conventional photolithographic method. For the sensor preparation, the Si/SiO_2 substrate was used and Au/Ti were deposited on top of the Si/SiO_2 wafer as a template with external electrodes or connections.

The schematic of a tripolar microelectrode sensor (figure 2) is illustrated as following. (1) The *cathode electrode* (figure 3(*a*)): an oxidized Si substrate was patterned by photolithographic method and etched to construct two micro-venthole structures with ∼5 × 3 mm^2 in area and ∼500 μm in thickness. The surface was deposited and patterned with Au/Ti thin film of 50 nm/270 nm in thickness and a vertically aligned SWCNTs film as field ionizer. The sensing film was deposited by screen and treated by Ar/O_2 plasma; the area and the average thickness of the film were ∼4 × 3 mm^2 and ∼20 nm, respectively. The cathode electrode was designed as a porous structure. Two micro-ventholes with ∼1 mm in each diameter were advantageous to electron diffusion and thermal conduction effects. As such, influential factors, such as sensor resolution and usage life, resulting from spatial involved electrons accumulation, were prevented to certain extent. (2) The *extraction electrode* (figure 3(*b*)): an oxidized Si substrate was etched into microtemplate of ∼200 μm in depth, then the electrode substrate was further patterned to form a row of holes with 500 μm in each diameter after the deposition of Au/Ti thin film. The extraction electrode lead the non self-sustaining discharge current of the sensor to electron collector. (3) The *electron collector electrode* (figure 3(*c*)): an oxidized Si substrate was etched into microditch structure of ∼480 μm in depth. The ditch field was selectively covered by a Au/Ti thin film. The electron collector was used to collect the resulting non self-sustaining discharge ionization current of gases between cathode and electron collector electrode by applying a desired voltage potential between respective electrodes. As a result, the gases exposed to sensor were ionized owing to the nanometer scale tip radius properties of SWCNTs.

As schematically shown in figure 3(*d*), the cathode and the extraction electrodes are biased with a positive voltage (U_1) and a negative voltage (U_2), respectively. The partial discharge current can be initiated if $U_1 > U_2$. The positive ion flow can be partially extracted from the cathode region toward the extraction electrode and be measured as electric current. The measurements were conducted using a picoammeter (Keithley 6485). Moreover, insulation (typically Si_3N_4) were used to separate the extraction from electron collector electrode, which provides a pinhole-free layer with low stress at room temperature and at temperatures below 350 °C, and also had high thermal shock resistance, high corrosion and wear resistance. Compared with other materials, Si_3N_4 is a good electrical insulator that can prevent electrical

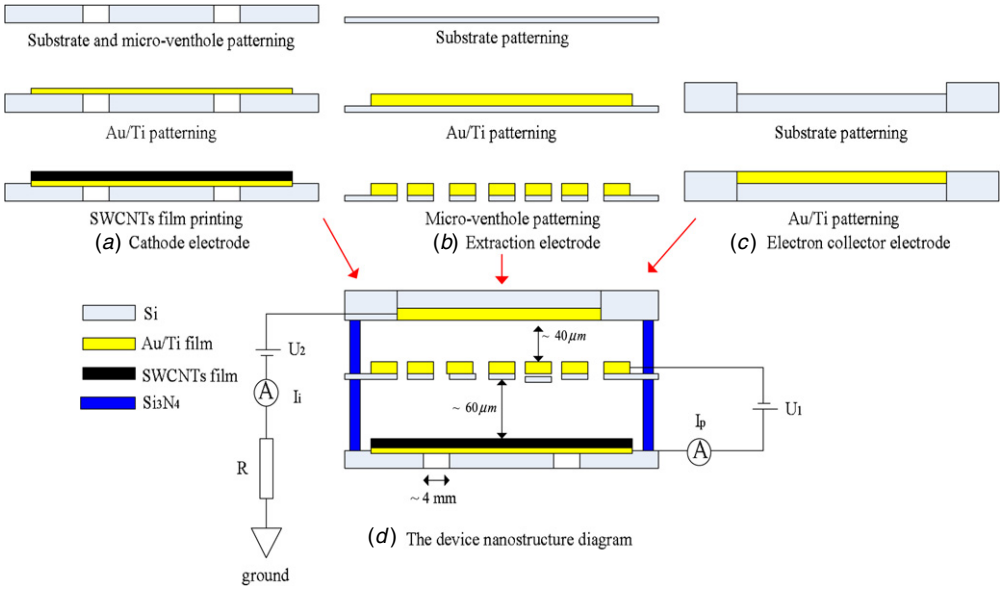

Figure 3. (*a*), (*b*), (*c*) are the fabrication processes of the field ionization cathode electrode, the extraction electrode, and the electron collector, repectively. (*d*) The device nanostructure diagram.

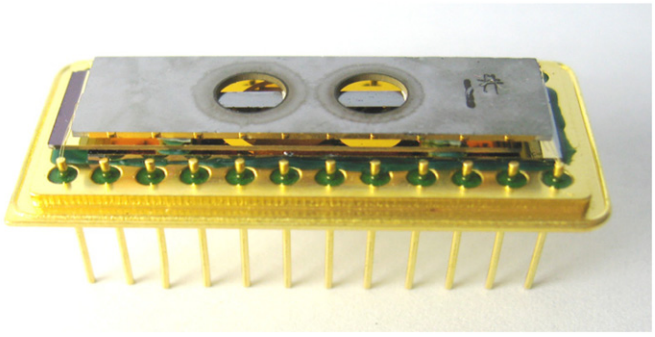

Figure 4. The sensor prototype device.

shortage between adjacent microelectrodes. The distance between interelectrodes could be adjusted in range of ∼30–250 μm by adjusting the thickness of the relevant electrical insulator.

The prototype apparatus after fabrication is showed figure 4.

3. Gas sensing properties and discussion

For gas sensing characterization, the fabricated electrodes were wire bonded to an external connection for testing. The sensor peripheral circuit was configured as follows: the extraction electrode was subjected to a 50 V dc power so that the voltage of the collector electrode was 10 V, while the cathode electrode was connected to the earth with a limiting current resistor. The value of the loading resistor was chosen to be as close as possible to the initial resistance of the sensor to optimize the resolution obtained from the measurement.

Figure 5 shows the schematic of the testing chamber used for testing the response to different gases. The device (figure 4) is placed inside the chamber, pumped to high vacuum and subsequently heated to 125 °C for ∼12 h prior to experiment. This process leads to the removal of already adsorbed gas molecules on the nanotubes surface.

The sensor was first exposed air to obtain the baseline, then to a desired concentration of measuring gas, and finally back to air which finished one experimental cycle. The flow rates of the testing gases were regulated by mass flow controllers.

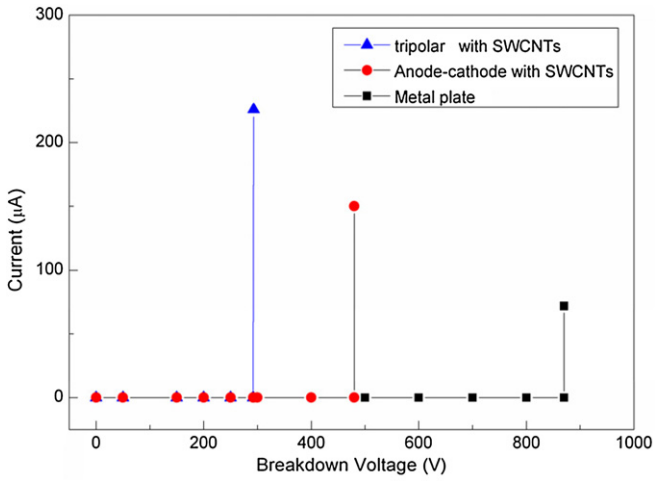

Figure 6. Current-voltage (*I*–*V*) curves for electrical breakdown.

The device was first tested in air under ambient pressure (figure 6) with the inter-electrodes distance between cathode, extraction and electron collector electrode are 40 μm and 60 μm, respectively. A continuous current discharge of ∼226 μA was generated utilizing SWCNTs as the field ionization cathode with tripolar on-chip microelectrode at ∼224 V. The same test was also carried by replacing the microtripolar sensor using SWCNTs with bipolar using SWCNTs and Cu plate. For the bipolar sensor, the breakdown voltage of air occurred at ∼480 V with a current discharge of ∼150 μA; however, for metal electrodes, the breakdown voltage of air occurred at ∼865 V with a current discharge of ∼75 μA. The results show that by introducing certain improvements into the electrode configuration of the miniaturized on-chip ionization gas sensors, compared with the conventional bipolar systems, the breakdown voltage of air was dramatically reduced. Besides that, the discharge current was also obviously increased, indicating the high sensitivity of sensors using SWCNTs as the field ionization cathode with tripolar microelectrode. This is because the extraction sensing electrode acts as the role of protuberances on the involvement of electron exchange between cathode and collector electrode. This facilitates electric field distribution uniform and speeds the occurrence of breakdown process.

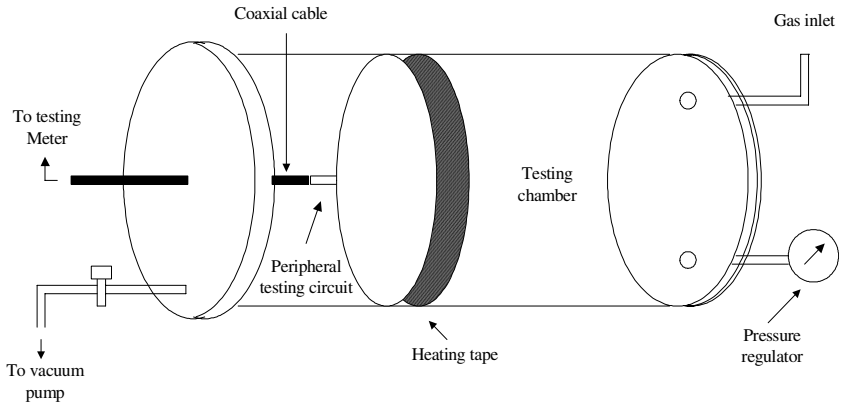

Figure 5. Schematic of the testing setup.

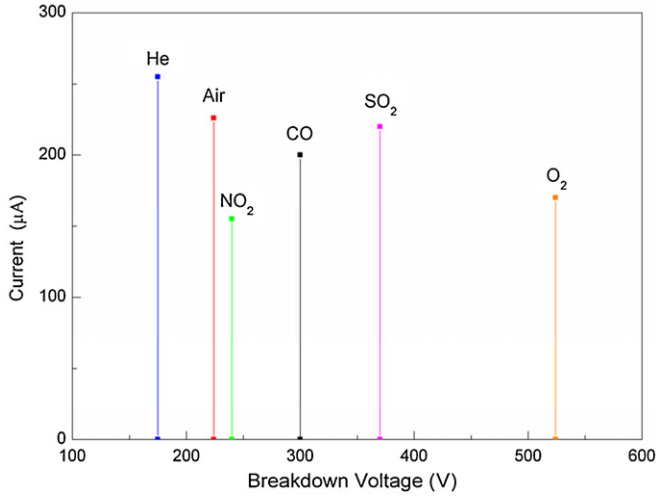

Figure 7. *I–V* curves for He, NO_2, CO, H_2, SO_2 and O_2, showing distinct breakdown voltages.

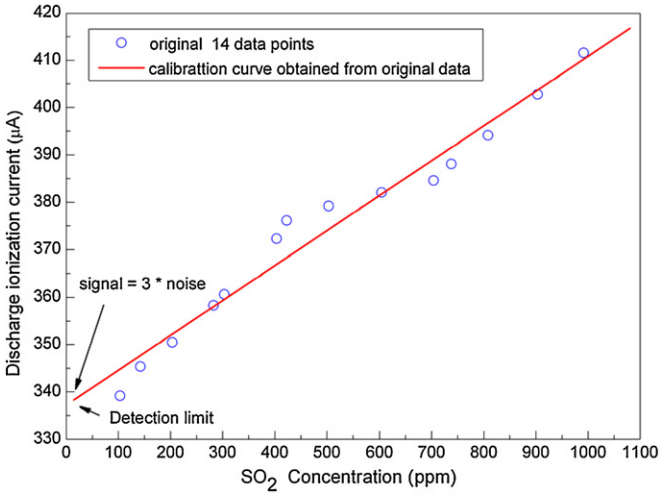

Figure 8. Relation between gas-concentrations and discharge current (29.1°C, 18.2%RH, 93.0 kPa).

The microtripolar sensor with SWCNTs film was used as the field ionization cathode to detect the identity of several gas species, such as He, NO_2, CO, H_2, SO_2 and O_2. Figure 7 showed the breakdown voltages of several gases at room temperature and at a chamber pressure of 10^3 Pa. It is notable that each gas displays a distinct electrical breakdown property: helium exhibits the lowest breakdown voltage (∼175 V) and O_2 shows the highest one (∼525 V). Obviously, this is a fingerprinting behavior. Each breakdown voltage is associated with one kind of gas.

To demonstrate the performance of the detection of trace amounts of different gases, here we show results from SO_2, a principal air pollutant, created by burning of sulfur-contaminated fossil fuels, and a corrosive and catalytic poison. Figure 8 shows the partial discharge current behavior of the nanosensor which was characterized the resulting non self-discharge ionization current as the function of the gaseous concentration. As can be seen from figure 8, the sensor response to SO_2 shows a good linear dependency with respect to concentration in the range investigated after the original discharge ionization were calibrated. However, the calibration error of the non self-sustaining discharge ionization, denoting δ_{cal}, is formulated as the ratio of the absolute value of the maximal calibrated aberration to the subtraction of the non self-sustaining discharge relating to concentration points 103.215 and 991.664 ppm, respectively:

$$\delta_{\text{cal}} = \frac{\Delta L_m}{Y_{\text{Fs}}} = \frac{5.2}{411.58 - 339.21} \times 100\% = 7.19\%$$

where ΔL_m presented the absolute value of the maximal calibrated aberration, and Y_{Fs} was the full-scale range of non self-sustaining discharge, i.e. the subtraction of the maximal and minimal discharge current.

In the above investigation, the lowest detectable concentration was limited by the present experimental setup. We can derive the detection limit from sensor's signal processing performance as described below.

The sensor noise can be calculated using the variation in the relative ionization current in the baseline using the root-mean-square deviation (rmsd) [17]. For example, we took 14 data points at the baseline before the SO_2 exposure. After plotting the data, a fifth-order polynomial fit, which provides not only the curve-fitting equation, but also the statistical parameters of the polynomial fit, was executed within the data-point range:

$$V_{\chi^2} = \sum_{i=1}^{14} (y_i - y)^2$$

where y_i is the measured data point and y is the corresponding value calculated from the curve-fitting equation. The rms noise is calculated as

$$\text{rms}_{\text{noise}} = \sqrt{\frac{V_{\chi^2}}{N}}$$

where N is the number of data points used in the curve fitting.

The sensor noise is 1.2299 for SO_2 sensor in figure 8. According to the IUPAC definition [18], when the signal-to-noise ratio equals 3, the signal is considered to be a true signal. Therefore, the detection limit can be extrapolated from the linear calibration curve when the signal equals 3 times the noise:

$$\text{DL(ppm)} = 3\frac{\text{rms}_{\text{noise}}}{\text{slope}}.$$

Using the above equation, the detection limit is calculated to be ∼0.5 ppm from the sensitivity of the sensor and the noise level. Therefore we conclude that the microtripolar sensor with SWCNTs film as the field ionization cathode is selective and can be used to detect trace amounts of different gases.

We have also carried out reproducibility studies for our tripolar microelectrode sensor with SWCNTs. More specifically, if the confidence level is 99.7% and confidence factor is 3, then the reproducibility of the sensor is 1.2%, which is comparable to and even better than that of metal oxide or polymer-based sensors [1, 3]. This indicates the excellent reproducibility of our tripolar microelectrode sensor with SWCNTs.

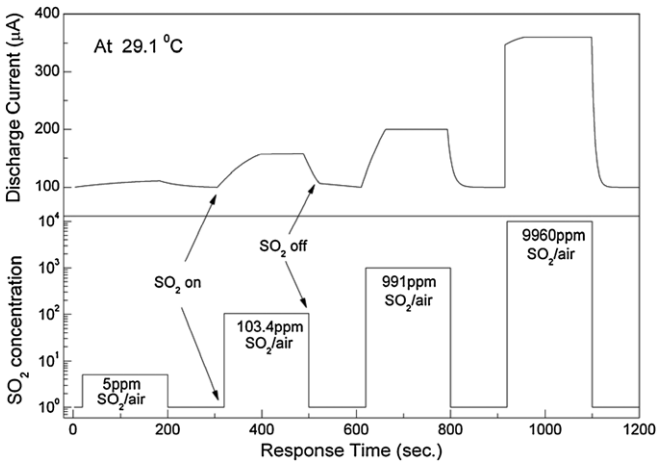

Figure 9. Room temperature dynamic responses of the studied sensor at different-concentration.

The dynamic response of the studied tripolar microelectrode sensor with SWCNTs under different concentration of SO_2 gases at room temperature is depicted in figure 9. When exposed to SO_2 gas, a quick SO_2-sensing reaction takes place, and the discharge ionization current increases rapidly to a final steady-state value. During the following time interval of 180 s with a constant SO_2 gas flow, the discharge ionization current maintains at this steady-state value. Then, after exposing to SO_2 gas, the synthetic air is introduced and the discharge ionization current drops quickly down to the original baseline. The response time τ_α, which is defined as the time of the discharge ionization current reaching the inverse exponential value (e^{-1}) of the final steady-state magnitude, is dependent on the initial rate of current variation. The corresponding value of τ_α is decreased from 120.4 to 20.95 s, while the concentration is increased from 5 to 9960 ppm. In comparison with other sensors [1], the studied device demonstrates much shorter response time.

4. Conclusions

In summary, this paper reports a gas sensor using single-walled carbon nanotubes as the field ionization cathode with the view of introducing certain improvements into the electrode configuration. The sensor has the merits of low cost and low breakdown voltage. The sharp tips of the nanotubes generate high electric fields at relatively low operating voltage, and show good sensitivity and selectivity. Further, the electrical response presents well-defined and reproducible linear behavior and a detection limitation of $<\sim$0.5 ppm for SO_2. More importantly, the stability and anti-oxidation of microtripolar sensors based SWCNTs are significantly better than the conventional bipolar electrodes sensor. Therefore, the simple, reliable, and reproducible sensor described here could be deployed for a variety of potential applications in the future.

Acknowledgments

Funding for the project was supported by National Natural Science Foundation of China under agreement no. 50877056 and China Postdoctoral Science Foundation China under agreement number no. 2011M501451.

References

[1] Cheng C C, Tsai Y Y, Lin K W, Chen H I, Hsu W H, Hung C W, Liu R C and Li W C 2006 Pd-oxide-$Al_{0.24}Ga_{0.76}As$ (MOS) high electron mobility transistor (HEMT)-based hydrogen sensor *IEEE Sensors J.* **6** 287–92

[2] Briand D, Krgoldss A, Van Der Schoot B, Weimar U and Barsan N 2000 Design and fabrication of high-temperature micro-hotplated for drop-coated gas sensors *Sensors Actuators* B **68** 223–33

[3] Zhang Y, Xu J Q, Xiang Q, Li H, Pan Q and Xu P C 2009 Brush like hierarchical ZnO nanostructures: synthesis, photoluminescence and gas sensor properties *J. Phys. Chem.* C **113** 3430

[4] Fedder G K, Howe R T and Liu T J K 2008 Techologies for cofabricating MEMS and electronics *Proc. IEEE* **96** 306–22

[5] Chan P C H, Yan G Z, Sheng L Y, Sharma R K and Tang Z 2002 An integrated gas sensor technology using surface micro-matching *Sensors Actuators* B **82** 277–83

[6] Ashish M, Nikhil K, Eric L, Bingqing W and Pulicket M A 2003 Miniaturized gas ionization sensors using carbon nanotubes *Nature* **24** 171–4

[7] Zhang Y and Liu J H 2002 Cross sensitivity reduction of gas using genetic neural network *Opt. Eng.* **41** 615–25

[8] Wang H, Zou C, Tian C, Zhou L, Wang Z and Fu D 2011 A novel gas ionization sensor using Pd nanoparticle-capped ZnO *Nanoscale Res. Lett.* **6** 534

[9] Zhang Y, Liu J H and Zhu C C 2010 Novel gas ionization sensors using carbon nanotubes *Sensor Lett.* **8** 219–27

[10] Pengfei Q, Ophir V, Mihai G, Ali J, Wang Q and Hongjie D 2003 Toward large arrays multiplex functionalized carbon nanotubes sensor for highly sensitive and selective molecular detection *Nano Lett.* **3** 345–51

[11] Wu R J, Chang W C, Tsai K M and Wu J G 2009 The novel CO sensing material CoOOH-WO3 with gold and SWCNT performance enhancement *Sensors Actuators* B **138** 35–41

[12] Kao P H, Dai C L, Hsu C C and Lee C Y 2009 Fabrication and characterization of a tunable in-plane resonate with low driving voltage *Sensors* **9** 2062–75

[13] Kong J, Soh H T, Cassell A M, Quate C F and Dai H 1998 Synthesis of individual single-walled carbon nanotubes on patterned silicon wafers *Nature* **395** 878–81

[14] Mark C H 2008 Progress toward mono-disperse single-walled carbon nanotubes *Nature Nanotech.* **3** 387–94

[15] Murakami Y, Iyauchi Y, Chiashi S and Aruyama S 2003 Direct synthesis of high-quality single-walled carbon nanotubes on silicon and quartz ubstrates *Chem. Phys. Lett.* **377** 49–54

[16] Cinke J M, Li J, Chen B, Cassell A, Delzeit L, Han J and Meyyappan M 2002 Pore structure of raw and purified HiPco single-walled carbon nanotubes *Chem. Phys. Lett.* **365** 69–74

[17] Martins H and Naes T 1998 *Multivariate Calibration* (New York: Wiley & Sons)

[18] Currie L A 1995 Nomenclature in evaluation of analytical methods including detection and quantification capabilities (IUPAC Recommendations 1995) *Pure Appl. Chem.* **67** 1699–723